9.6 SIMULATIONS OF AEROSOL-CLOUD-DYNAMICAL FEEDBACKS RESULTING FROM ENTRAINMENT OF AEROSOL INTO THE MARINE BOUNDARY LAYER DURING ASTEX

Hongli Jiang[1], Graham Feingold[2], and William R. Cotton[1]

[1]Department of Atmospheric Science, Colorado State University Fort Collins, Colorado

[2]NOAA, Environmental Technology Laboratory, Boulder, Colorado

April 2, 2002

1 INTRODUCTION

The purpose of this paper is to consider the effect of entrainment of long range transported aerosol into the subtropical marine boundary layer. We address several key questions: (1) what is the effect of entrainment of polluted air at cloud top on the marine boundary layer structure and optical properties? (2) will the fact that entrainment of polluted aerosol and drier, warmer free-tropospheric air occur simultaneously, enhance or diminish the primary aerosol indirect effect?

To address these issues, a number of numerical simulations were performed in a two-dimensional eddy-resolving model (ERM) of the Regional Atmospheric Modeling System (RAMS) with liquid-phase, bin-resolving microphysics (Feingold *et al.*, 1996). A thermodynamic sounding taken from the island of Santa Maria on 17 June 1992 is used for all the simulations. This day was chosen because it lies between the Lagrangian 1 and Lagrangian 2 during ASTEX when polluted air was being transported to the clean MBL.

2 EXPERIMENT DESIGN

Two baseline simulations are performed. The first has a constant initial CCN profile of 100 cm^{-3} (hereafter referred to as N100-D3). In the second baseline simulation, the initial CCN profile retains a value of 100 cm^{-3} in the MBL but jumps to 1200 cm^{-3} at cloud top (hereafter referred to as N1200-D3). This profile is roughly based on CCN data collected during ASTEX research (Fig.1).

[1]Corresponding author address: Hongli Jiang, Department of Atmospheric Science,Colorado State University, Ft. Collins, CO 80523,
e-mail: jiang@atmos.colostate.edu

Large-scale subsidence is prescribed by $w_s = -D \times z$. Where D is the mean horizontal divergence between the surface and the marine inversion, and z is the model height in m. To investigate the sensitivity of the simulated MBL to large-scale subsidence, we repeated the two baseline simulations (N100-D3 and N1200-D3) with various degrees of large-scale subsidence by changing D from zero to 3×10^{-6} s^{-1}. The experiments are summarized in Table 1.

Due to spatial limitation, we only show a few selected figures from the two baseline simulation ($D = 3 \times 10^{-6} s^{-1}$). More results will be presented at the conference, and appear in the publication (Jiang *et al.*, 2002).

3 SIMULATION RESULTS

The layer-averaged liquid water mixing ratio for the N100-D3 run (Fig. 2) shows a solid stratocumulus layer for the entire simulation, while a penetrating cumulus cell rises up from the subcloud layer into the stratocumulus at ~300 min, a feature often observed in the ASTEX cumulus transition regime. In the N1200-D3 run (figure not shown) the penetrating cumulus convection exists but is much weaker. The cumulus and stratocumulus are in two separate layers.

In the N100-D3 run, the maximum cloud-base drizzle rate (Fig. 3a) of 0.5 mm day^{-1} occurs around 300 min, and about the same time as the cumulus penetration. The time series of column maximum $\sigma_w = (w'w')^{1/2}$ (Fig. 3b) shows that maxima in σ_w correspond to the deeper cloud and higher cloud-base drizzle rate, indicating a stronger dynamic response during and immediately after the higher drizzle events at cloud base. It appears that evaporation of drizzle just below cloud base produces

a cooler and moister layer which is sufficient to destabilize the subcloud layer (not the entire boundary layer) and enhance the strength of penetrating cumulus (e.g. Paluch and Lenschow, 1991; Feingold et al., 1996). The penetrating cumulus supplies more surface water vapor and helps maintain and enhance the LWP (Fig. 3c).

In the N1200-D3 run, however, the cloud-base drizzle rate is only one fifth of that in the N100-D3 run. The increased droplet number in the N1200-D3 run suppresses drizzle formation and cloud base drizzle rates are substantially lower than for N100-D3. Penetrating cumulus are much weaker and LWP much lower (Fig. 3c).

The role of evaporative cooling just below cloud base in enhancing cumulus convection is investigated further by examining the vertical structure of various variables, horizontally and time-averaged over the sixth hour.

Drizzle (Fig. 4) is mainly in the cloud layer with only 3% present below the cloud base in the N100 run, but none reaching the surface for either runs. Evaporation of drizzle will cool and moisten the layer below the cloud base in the N100-D3 run.

$d\theta/dz$ (Fig. 5) provides evidence that the cooling from evaporating drizzle induces destabilization with respect to the surface in the layer between 550 - 700 m. The destabilizing effect only applies to the case when drizzle evaporates completely before reaching the surface (e.g., Paluch and Lenschow, 1991; Feingold *et al.*, 1996). Paluch and Lenschow (1991) differentiated between two scenarios: (i) precipitation reaches the surface and the associated cooling tends to *stabilize* the entire layer below the cloud; and (ii) precipitation evaporates just below cloud and the associated cooling tends to *destabilize* the layer below cloud. The case under discussion clearly corresponds to the latter. To further strengthen our case that small amounts of drizzle evaporating near cloud base can destabilize the boundary layer, the simulation of N100-D3 was repeated with the initial CCN concentration reduced to 20 cm^{-3}. Drizzle reaches the surface (figure not shown) and does not lead to formation of cumulus under stratus as expected.

The entrainment rate w_e is normally computed as the average $dz_i/dt - w_s$, where z_i is the local height of the inversion. The case under discussion has a very weak inversion, which makes it very difficult to compute the entrainment rate based on the q_t jumps. Following Moeng *et al.*, (1999), the mean cloud-top height z_t is calculated, and hence dz_t/dt. The entrainment rate is defined as $w_e = dz_t/dt - w_s$. The growth rate of the cloud-top height, and w_e averaged over the last six hours of simulation are shown in Table 2. Comparison between the N100-D3 and N1200-D3 shows that the cloud top grows slightly faster in the N1200-D3 run than it does in the N100-D3 run. Drizzle at cloud base may not remove water from cloud effectively, but the warming at the cloud top reduces the net cooling resulting in less entrainment in the N100-D3 run.

4 DISCUSSION

The role of penetrating cumulus in supplying stratocumulus cloud moisture in the warm ocean regime is well known and these results have exemplified the extent to which this process is sensitive to variations in aerosol concentration. Although neither of the baseline simulations can be characterized as drizzling cases, small amounts of drizzle evaporating beneath cloud base in the clean case (N100-D3) strengthen cumulus transports relative to the case with the elevated pollution layer (N1200-D3). The result is a significantly enhanced LWP for N100-D3 (Fig. 3c). In terms of the effect of the elevated pollution layer on cloud albedo, the two effects tend to counter one another. The first is an enhancement in albedo as a result of entrainment of air rich in CCN into the cloud (e.g. Duda *et al.*, 1996). The second is a suppression of LWP due to weaker penetrating cumulus. On balance, the cloud albedo is hardly changed for a significant portion of the simulation (300 min – 460 min, Fig. 3d). Between 100 – 300 min, and 460 – 600 min, the enhanced droplet concentrations in N1200-D3 tip the scales in the direction of higher albedo, albeit at a level reduced from what would be expected from the primary "Twomey Effect" where albedo enhancement is considered at constant LWP. The dynamical feedback has therefore acted to minimize the classical aerosol indirect effect.

5 SUMMARY

The two baseline simulations study the response of the modeled marine boundary layer to the change in CCN concentration. As the polluted air (higher N_{ccn}) is entrained into the cloudy boundary layer, droplet number N_d increases and effective radius decreases. However, due to a subtle feedback to boundary layer dynamics, penetrating cumulus convection is weakened and LWP is significantly reduced. The result is that on balance, cloud albedo is not significantly affected by the entrained pol-

luted air. The classical primary aerosol indirect effect whereby enhanced aerosol concentrations result in higher droplet concentrations and more reflective clouds is therefore minimized.

The mechanism responsible for stronger penetrating cumulus in the lower N_{ccn} case is identified. It is shown that the presence of small amounts of drizzle evaporating just below cloud base destabilizes this region with respect to the surface. This should be contrasted with situations where drizzle falls to the surface and the associated cooling stabilizes the entire boundary layer (Paluch and Lenschow, 1991; Feingold *et al.,* 1996).

The results presented here have demonstrated that dynamical feedbacks associated with entrainment of polluted air into the MBL may either reduce or enhance the aerosol indirect effect, depending on the large-scale synoptic conditions. Although the results are case specific, they do indicate that, in general, quantification of the aerosol indirect effect presents a formidable challenge.

Acknowledgments. This research was supported by grants from the NSF under Grant ATM-9904128. The observational data used in this study were obtained from the NASA Langley Research Center Atmospheric Sciences Data Center.

6 REFERENCE

Duda, D. P., G. L. Stephens, B. Stevens, and W. R. Cotton, 1996: Effects of aerosol and horizontal inhomogeneity on the broadband albedo of marine stratus: numerical simulations, *J. Atmos. Sci., 53*, 3757–3769.

Feingold, G., B. Stevens, W. R. Cotton, and A. S. Frisch, 1996: The relationship between drop in-cloud residence time and drizzle production in numerically simulated stratocumulus clouds, *J. Atmos. Sci., 53*, 1108–1122.

Jiang, H., G. Feingold, and W. R. Cotton, 2002: Simulations of aerosol-cloud-dynamical feedbacks resulting from entrainment of aerosol into the marine boundary layer during ASTEX, *J. Geophys. Res.*, In Press.

Moeng, C-H, P. P Sullivan, and B. Stevens, Including radiative effects in an entrainment rate formula for bouyancy-driven PBLs, *J. Atmos. Sci., 56*, 1031–1049, 1999.

Paluch, I. R, and D. H. Lenschow, Stratiform cloud formation in the marine boundary layer, *J. Atmos. Sci., 48*, 2141–2158, 1991.

Table 1: Description of experiments

EXP	CCN_{max} (cm^{-3})	D (s^{-1})	w_s (cm s^{-1})
N100-D0	100	D=0.0E-6	0.0
N100-D1	100	D=1.0E-6	-0.14
N100-D2	100	D=2.0E-6	-0.28
N100-D3	100	D=3.0E-6	-0.42
N100-D4	100	D=4.0E-6	-0.56
N1200-D0	1200	D=0.0E-6	0.0
N1200-D1	1200	D=1.0E-6	-0.14
N1200-D2	1200	D=2.0E-6	-0.28
N1200-D3	1200	D=3.0E-6	-0.42
N1200-D4	1200	D=4.0E-6	-0.56

Table 2: The growth rate of the cloud-top height averaged over the last six hour of simulation

N100-D3		N1200-D3	
dz_t/dt cm s^{-1}	w_e cm s^{-1}	z_t/dt cm s^{-1}	w_e cm s^{-1}
0.930	1.271	0.962	1.308

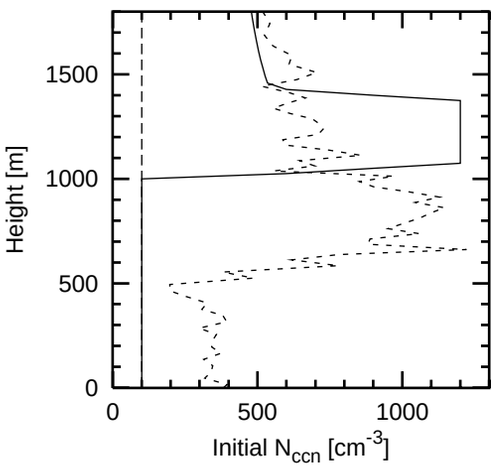

Figure 1: Vertical profile of the initial CCN used for the N1200-D3 run (solid line), the CCN profile observed during Research Flight 10 of ASTEX, activated at 0.8% supersaturation (short-dashed line), and the constant initial CCN used for the N100-D3 run (long-dashed vertical line).

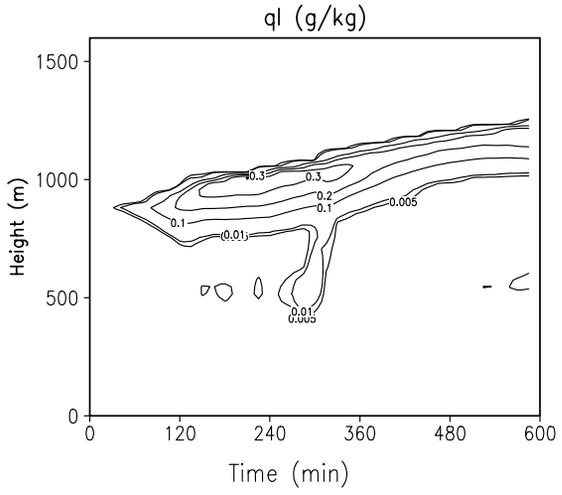

Figure 2: Time-height cross section of liquid water mixing ratio q_l (the first contour is 0.005 g kg^{-1}, the second contour is 0.01 g kg^{-1}, and the contour interval is 0.1 g kg^{-1} thereafter) for the N100 run.

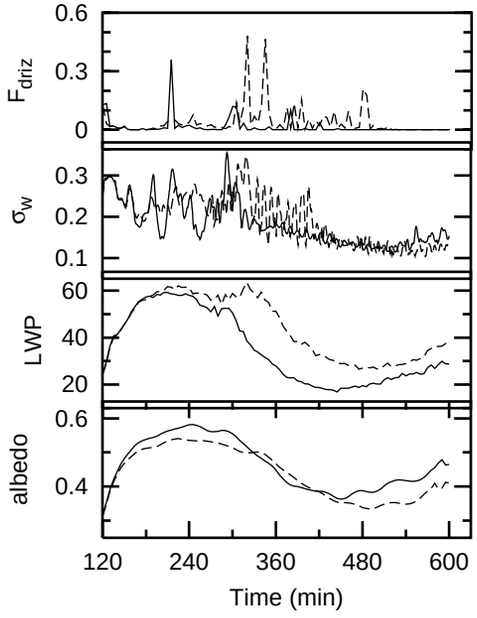

Figure 3: The temporal evolution of (a) cloud-base drizzle rate F_{driz} (mm day^{-1}), (b) maximum value of $< w'w' >^{1/2}$ labeled as σ_w (m s^{-1}), (c) LWP (gm^{-2}), and (d) albedo. The solid line denotes the N1200-D3 run and the dashed line denotes the N100-D3 run.

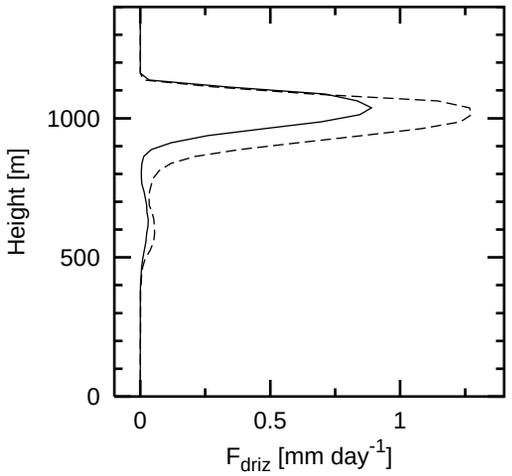

Figure 4: Horizontally averaged drizzle rate profile time averaged over the sixth hour of the simulation for both the N1200-D3 and N100-D3 run with line types as indicated in Fig. 3.

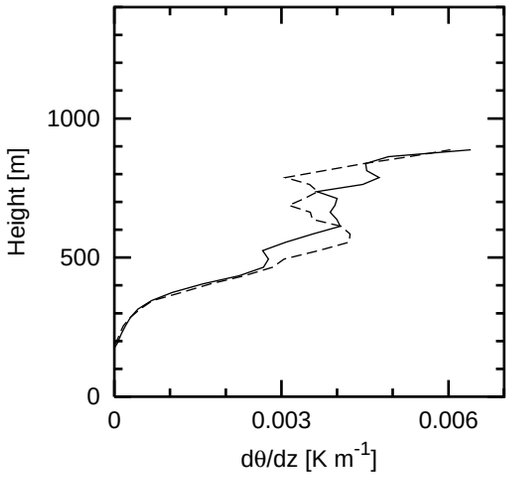

Figure 5: Horizontally averaged profile of lapse rate $d\theta/dz$ time averaged over the sixth hour of the simulation for both the N1200-D3 and N100-D3 run with line types as indicated in Fig. 3.